APP Template V1.70 Article id: nanoaa7589 Typesetter: MPS Date received by MPS: 31/05/2017 PE: MAC004070 CE: LE:

IOP Publishing Nanotechnology

Nanotechnology **00** (2017) 000000 (7pp)

Effect of polymer residues on the electrical properties of large-area graphene–hexagonal boron nitride planar heterostructures

Yijing Y Stehle[1], Dmitry Voylov[2], Ivan V Vlassiouk[1], Matthew G Lassiter[1], Jaehyeung Park[1], Jaswinder K Sharma[1], Alexei P Sokolov[2,3] and Georgios Polizos[1]

[1] Energy & Transportation Science Division, Oak Ridge National Laboratory, Oak Ridge, TN 37831, United States of America
[2] Department of Chemistry, University of Tennessee, Knoxville, TN 37996, United States of America
[3] Chemical Sciences Division, Oak Ridge National Laboratory, Oak Ridge, TN 37831, United States of America

E-mail: polyzosg@ornl.gov

Received 25 February 2017, revised 16 May 2017
Accepted for publication 30 May 2017
Published DD MM 2017

Abstract

Polymer residue plays an important role in the performance of 2D heterostructured materials. Herein, we study the effect of polymer residual impurities on the electrical properties of graphene–boron nitride planar heterostructures. Large-area graphene (Gr) and hexagonal boron nitride (h-BN) monolayers were synthesized using chemical vapor deposition techniques. Atomic van-der-Waals heterostructure layers based on varied configurations of Gr and h-BN layers were assembled. The average interlayer resistance of the heterojunctions over a 1 cm^2 area for several planar heterostructure configurations was assessed by impedance spectroscopy and modeled by equivalent electrical circuits. Conductive AFM measurements showed that the presence of polymer residues on the surface of the Gr and h-BN monolayers resulted in significant resistance deviations over nanoscale regions.

Supplementary material for this article is available online

Keywords: graphene, hexagonal boron nitride, heterostructures, interlayer resistance, impedance

SQ1 (Some figures may appear in colour only in the online journal)

Introduction

The design of atomically thin electronic devices requires the synthesis and assembly of large-area heterostructures of two-dimensional (2D) crystals with complementary electrical properties and compatible crystal structures. Graphene (Gr) and hexagonal boron nitride (h-BN) are the most commonly used 2D crystals with intrinsic electrical conductive and insulating properties, respectively. Because of the similar lattice parameters of the Gr and h-BN, the latter is an ideal dielectric support layer for the fabrication of Gr-based nanoelectronics and devices for energy storage [1–6]. The charge carrier mobility in planar heterostructures of atomic layer Gr that is either supported by h-BN or being encapsulated between h-BN atomic layers has been shown to significantly increase due to the reduced surface roughness, screening of surface charges and the weaker electron-phonon surface scattering [7–9]. The reported micrometer-scale mobility values of the Gr/h-BN heterostructures are approximately one order of magnitude higher than the respective values of the Gr transferred onto oxidized silicon wafer substrates [9].

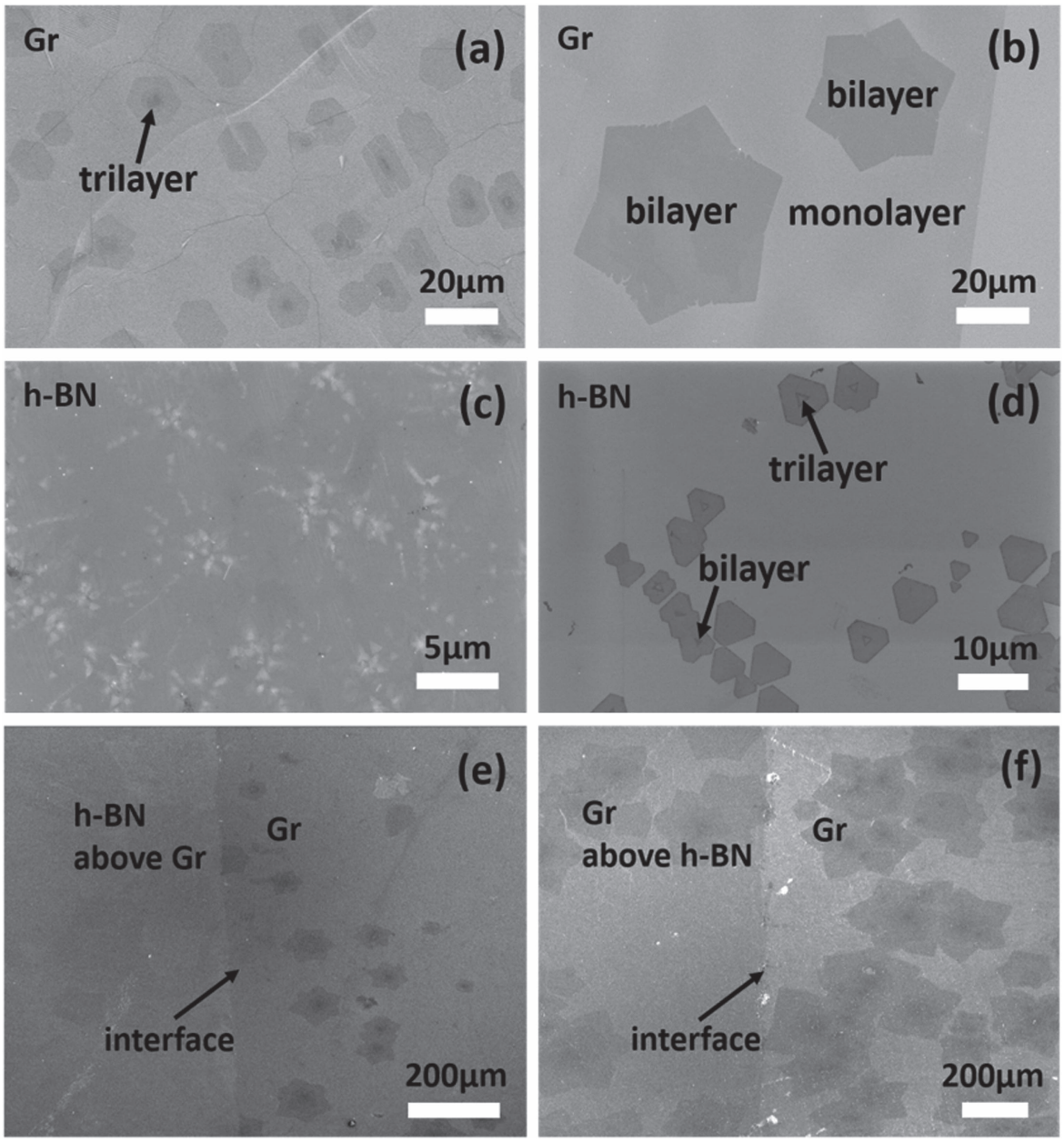

Figure 1. SEM images of mono-, bi-, and tri- layers of Gr (a), (b) and h-BN (c), (d) crystals on SiO_2/Si substrate. The assembled heterostructures of h-BN/Gr and Gr/h-BN are shown in images (e) and (f), respectively.

Chemical vapor deposition (CVD) is the predominant technique for growing scalable quantities of Gr and h-BN single layers on copper catalyst substrates. Polymer sacrificial layers, such as poly(methyl methacrylate) (PMMA), have commonly been used to remove the Gr and h-BN layers from the copper foil and to assemble them into van-der-Waals heterostructures on the substrate of choice. The latter, are typically annealed at temperatures higher than 500 °C to remove the PMMA; however, the complete removal of the PMMA residue is still a challenging problem [10–12] and it has been shown to impact the electrical properties of the Gr [13, 14]. Moreover, the configuration of multilayer heterostructures introduces additional capacitive contributions due to the dielectric layers [2, 15, 16]. Herein, we investigate the electrical properties of large area (1 cm^2) multilayer configurations of Gr and h-BN planar structures and the effect of the PMMA residues on the electrical properties. The electrical characterization was performed using impedance spectroscopy, and current–voltage (I–V) measurements using conductive atomic force microscopy (AFM). Scanning electron microscopy (SEM), and Raman spectroscopy were utilized to characterize the quality of the synthesized 2D crystals and their lateral heterostructures.

Experimental

Gr and h-BN monolayers were grown on copper foils using the regular CVD technique and transferred on the substrate via the wet chemical method. The growth conditions, the

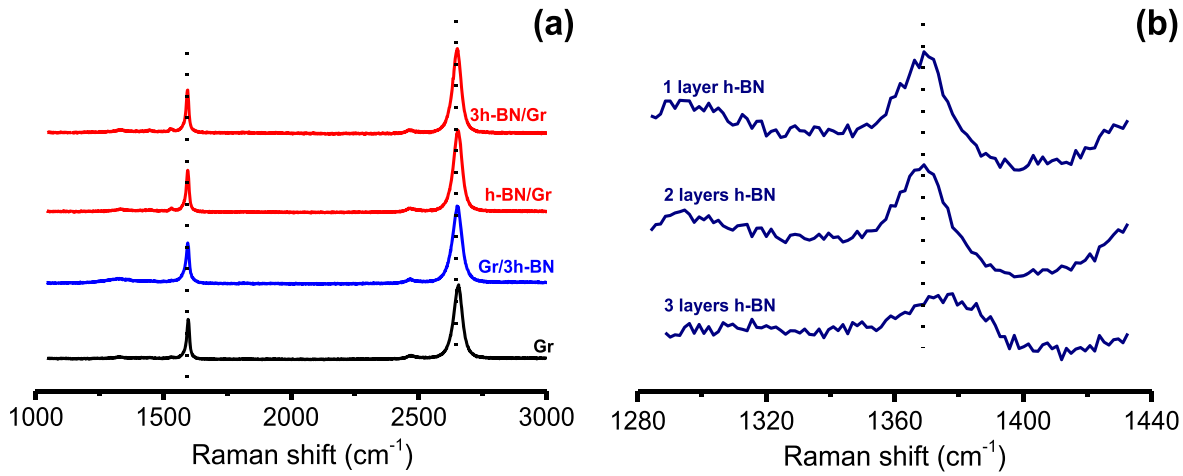

Figure 2. Raman spectra of (a) Gr and Gr/h-BN heterostructures and (b) h-BN layers. All configurations were synthesized using CVD and assembled using layer-by-layer techniques. The intensity of the h-BN band in (a) is masked by the strong Gr band.

crystal morphology and the transfer process of the Gr and h-BN layer onto substrates are described elsewhere [17, 18]. Details on the experimental setup are provided in the supplementary data section is available online at stacks.iop.org/NANO/0/000000/mmedia.

Results and discussion

The SEM images of the CVD synthesized h-BN and Gr are shown in figures 1(a)–(d). During the growth of the Gr and h-BN, the crystal domains keep growing till coalesced to form a continuous monolayer film. Intermittent bi- and tri- layer crystals were randomly formed on the top of the monolayer film. The synthesized layers were assembled at several configurations to form heterostructured layered films. Representative SEM images of the h-BN/Gr, and Gr/h-BN configurations are shown in figures 1(e) and (f), respectively. Raman spectra of the h-BN and Gr layers were obtained over several spots to verify the complete coverage of the films and the number of single crystal layers. Representative Raman spectra are shown in figure 2. The characteristic peak for a single h-BN layer was found at 1369 cm^{-1} (figure 2(b)) [18–20]. The characteristic G and 2D bands approximately at 1590 and 2650 cm^{-1}, respectively for the single layer Gr are shown in figure 2(a) [21–23]. Defects in the crystal structure may form during the growth and assembly process. They are associated with the formation of grain boundaries, lattice distortions, surface wrinkles, and dangling bonds; all of which impact the macroscopic electrical properties [24–27]. The intensity of the D band at 1350 cm^{-1} which is associated with the formation of crystal defects is very weak in the measured spectra (figure 2(a)) indicating the high quality of the assembled layers.

The assembly of the heterostructures is a multi-step process. Single layers of Gr and h-BN were synthesized on copper foil and were spin coated with PMMA. After dissolving the copper, the PMMA-coated single layers were thoroughly rinsed with deionized water and transferred onto the silicon wafer. The transferred layers were rinsed with acetone and isopropyl alcohol, and subsequently were annealed at 550 °C for 30 min (h-BN was annealed in vacuum whereas Gr was annealed in CO_2) to remove the PMMA residues [18, 28]. The surface morphologies of the transferred layers according to AFM measurements, are shown in figure 3. After rinsing with acetone, the PMMA residues are still substantial and they cover almost the entire Gr surface. The height of the PMMA features varies from 25 to 45 nm (figures 3(a) and (b)). The annealing resulted in a significant reduction of the residue amount. Large size (~20 nm height) residues are scattered on the Gr surface. The average residue height has been decreased to approximately 5–10 nm.

Impedance spectroscopy and conductive AFM measurements were carried out to measure the interlayer electrical properties of the heterostructures. The impedance measurements provided the frequency dependence of the distributed (average values over the length scales of the assembled circuits) interlayer resistance and capacitance; whereas, AFM measurements were used to map the local resistance and probe variations in the resistance values due to the PMMA residues. To measure the interlayer electrical properties of the heterostructures, three, six, and twelve single layers of h-BN were layer-by-layer assembled between single Gr layers (Gr/3h-BN/Gr, Gr/6h-BN/Gr, and Gr/12h-BN/Gr). A reference sample of two Gr layers (Gr/Gr) was also assembled to measure the resistance and capacitance contributions of the Gr electrodes. The area of the heterostructures was 1 cm^2. The frequency dependence of the impedance and phase angle, and the equivalent circuit used to simulate the electrical response of the layered structures are shown in figures 4(a) and (b), respectively. The resistance of the Gr electrodes is denoted as R_{elect}. A combination of parallel *R*–*C* configurations was used to simulate the distributed heterojunction resistance and capacitive contributions in the layered assembly. Specifically,

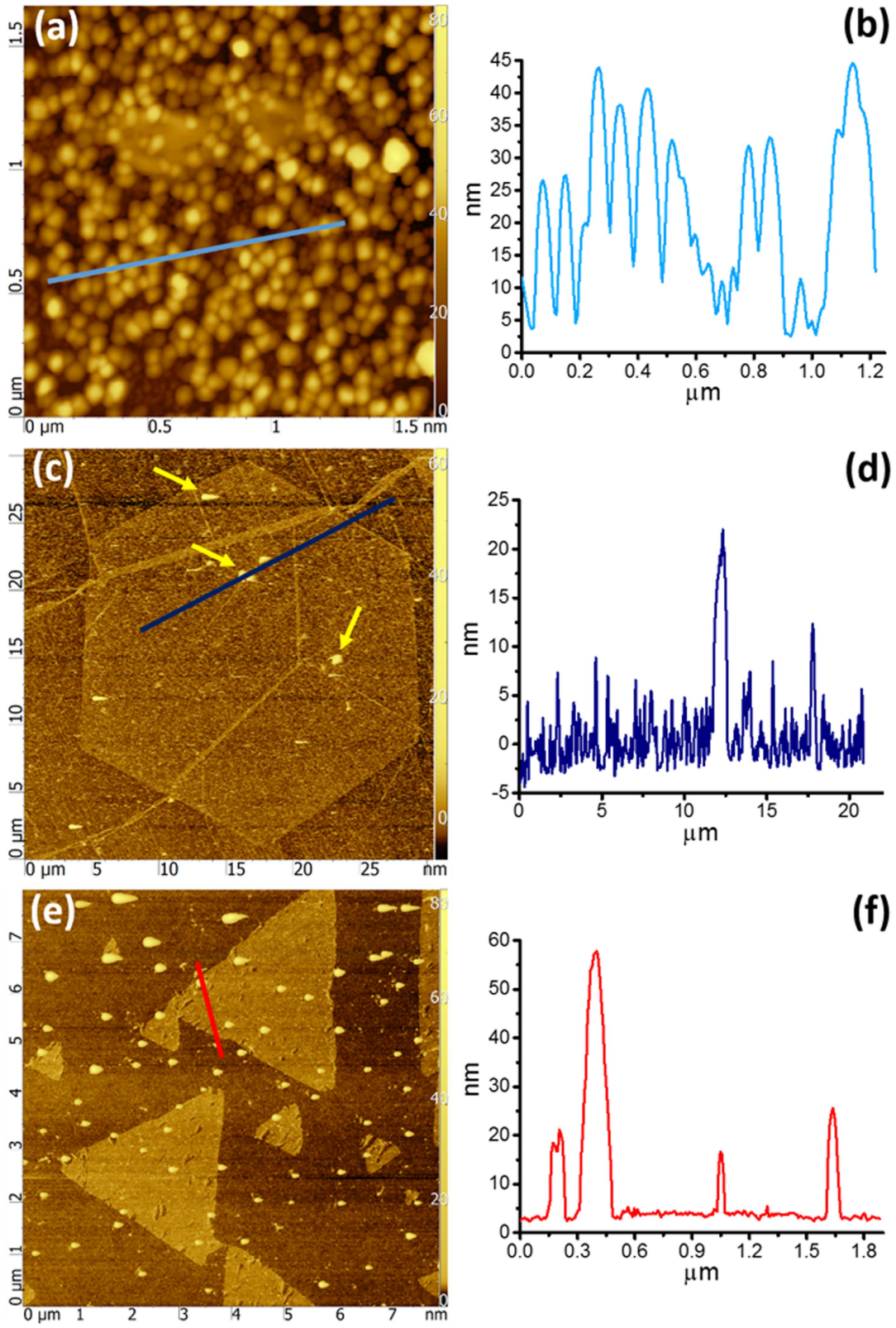

Figure 3. AFM images and surface profiles according to line scans of Gr and h-BN single layers spin coated with PMMA. (a), (b) Gr/PMMA after rinsing with acetone. (c), (d) Gr/PMMA after annealing at 550 °C. The arrows indicate large size PMMA residues. (e), (f) h-BN/PMMA after annealing at 550 °C. The measurements were performed on Si wafers with a top layer of 100 nm SiO_2. The roughness of the substrate is less than 1 nm.

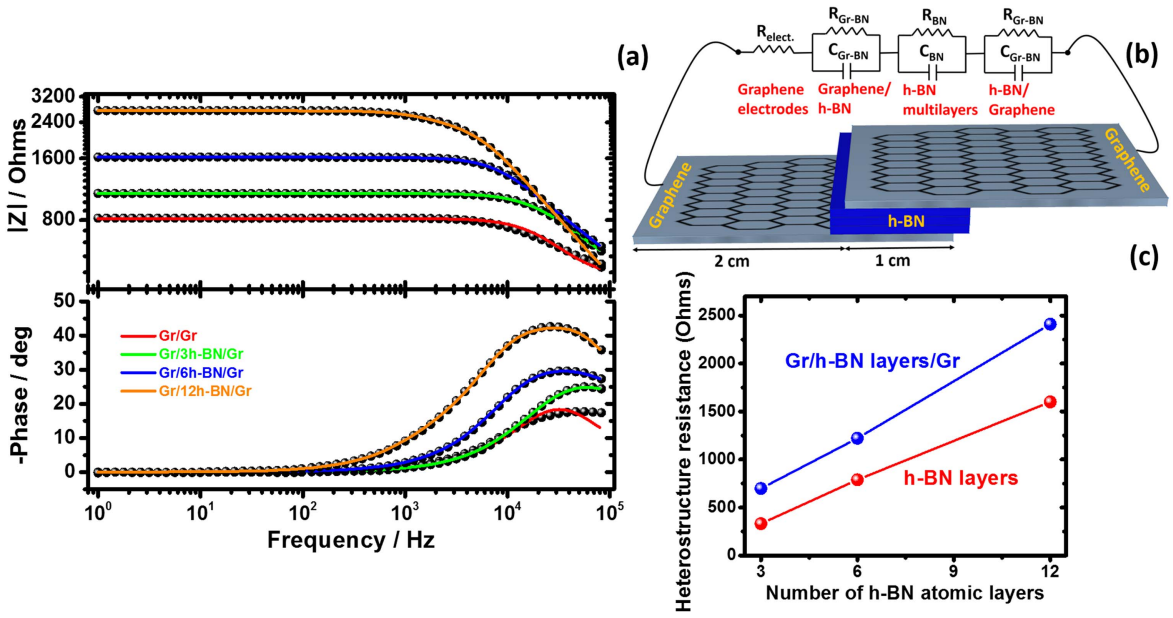

Figure 4. (a) Bode plot for the frequency dependence of the impedance and phase angle for the layered configurations indicated on the plot. The lines are the best fits of the simulated circuit to the experimental data. The equivalent circuit is shown in (b). (c) The summarized resistance values.

R_{BN} and C_{BN} correspond to the contributions of the BN layers; whereas, $R_{Gr\text{-}BN}$ and $C_{Gr\text{-}BN}$ correspond to the Gr electrode and BN interlayer connections. All parameters in figure 4(b) were allowed to vary without constraints during the fitting iterations. For all sample configurations, the R_{elect} and $R_{Gr\text{-}BN}$ values were found to vary from 320 to 420 Ω. The interlayer resistance values R_{BN} were found to systematically increase when increasing the number of h-BN layers. The R_{BN} values for the Gr/3h-BN/Gr, Gr/6h-BN/Gr, and Gr/12h-BN/Gr layer configurations are 330, 790 and 1600 Ω, respectively. The resistance values of the layered h-BN assembly, as well as of the entire heterostructure (including the $R_{Gr\text{-}BN}$ resistance values between the h-BN layers and the top and bottom electrode) are summarized in figure 4(c). The simulated capacitance values in figure 4(b) vary from 10 to 40 nF. These rather low values correspond to an approximate thickness of 100 nm for the assembled nanostructures. The latter, as well as the absence of electron tunneling can be attributed to the PMMA residues between the h-BN layers.

AFM equipped with a conductive tip ~~of approximately 30 nm radius~~ was used to map the *I*–*V* curves over nanoscale regions for the Gr, h-BN, and h-BN/Gr configurations. The local resistance values for all configurations were found to vary significantly due to the PMMA residues. Representative resistance map images are shown in figure 5.

The resistance values were calculated from the slope of the *I*–*V* curves and were found to typically vary from several hundred Ω–20 kΩ for the single Gr layer. Broad variations in the resistance values of the single h-BN layer and the h-BN/Gr heterostructure were also observed. The typical resistance values were approximately 80 kΩ.

Conclusions

Atomic layers of h-BN and Gr were grown on copper foils using CVD techniques. PMMA was used to transfer the single layers and assemble them into van-der-Waals heterostructures of three, six and twelve h-BN layers that are encapsulated between Gr electrodes. The heterostructures were annealed at 550 °C to remove the PMMA and their interlayer electrical properties were measured. The resistance values of the assembled single layers varied from several hundred Ω to tens of kΩ over nanometer size areas. This enormous variation is attributed to the PMMA residues that are present between the assembled monolayers. The approximate size of the PMMA residues is 5–10 nm resulting in high interlayer resistance and poor electrical contact between the assembled layers.

Acknowledgments

This research was supported by the Laboratory Directed Research and Development Program of ORNL, managed by UT-Battelle, LLC, for the US Department of Energy, and the US Strategic Environmental Research and Development Program (SERDP) under contract WP-2524. DV and APS acknowledge partial financial support by the US Department of Energy, Office of Science, basic Energy Sciences and Engineering Division. A portion of this research was conducted at the Center for Nanophase Materials Sciences, which is sponsored at Oak Ridge National Laboratory by the Scientific User Facilities Division, US Department of Energy. The Oak Ridge National Laboratory is operated for the US

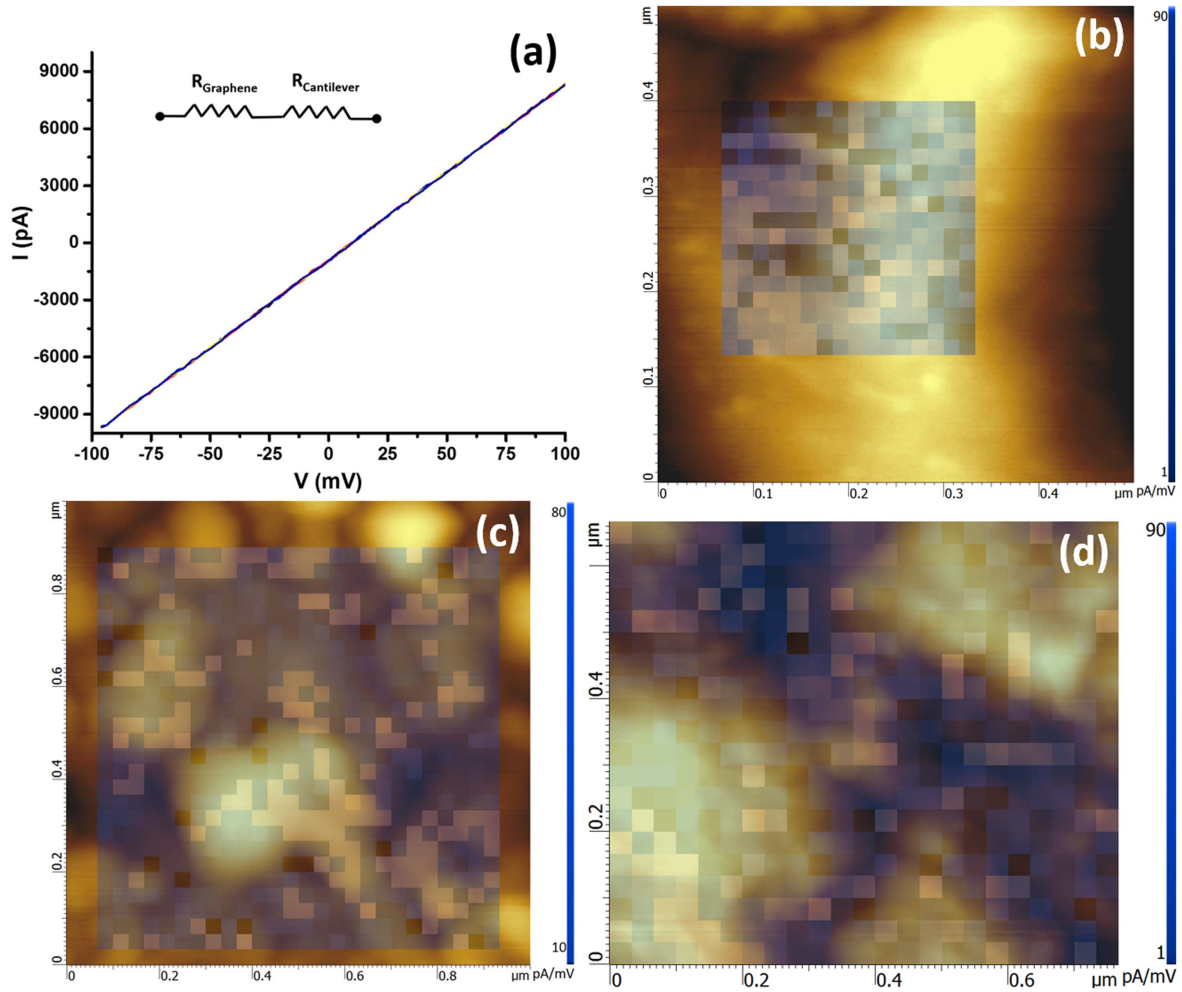

Figure 5. Conductive AFM measurements of a single Gr layer, a single h-BN layer, and a h-BN/Gr bilayer. All configurations were mounted on a silicon wafer that was sputtered with 100 nm silver. (a) Representative *I–V* curves and the equivalent circuit that was used to calculate the resistance of the Gr layer (R_{Graphene}). A 10.8 MΩ resistor ($R_{\text{Cantilever}}$) is connected to the AFM probe. Surface resistance map of the (b) single Gr layer, (c) single h-BN layer, and (d) h-BN/Gr bilayer. The colored pixels correspond to measured areas with different *I–V* slopes. The dark pixels correspond to non-conductive areas with resistance values in the MΩ range.

Department of Energy by UT-Battelle under contract no. DE-AC05-00OR22725.

Notes

The authors declare no competing financial interest.

Notice of copyright

References

[1] Zhao Y, Wan Z, Xu X, Patil S R, Hetmaniuk U and Anantram M P 2015 Negative differential resistance in boron nitride graphene heterostructures: physical mechanisms and size scaling analysis *Sci. Rep.* **5** 10712
[2] Kretinin A V *et al* 2014 Electronic properties of graphene encapsulated with different two-dimensional atomic crystals *Nano Lett.* **14** 3270–6
[3] Shirodkar S N and Kaxiras E 2016 Li intercalation at graphene/hexagonal boron nitride interfaces *Phys. Rev.* B **93** 245438
[4] Shi G *et al* 2014 Boron nitride–graphene nanocapacitor and the origins of anomalous size-dependent increase of capacitance *Nano Lett.* **14** 1739–44

[5] Bruzzone S, Logoteta D, Fiori G and Iannaccone G 2015 Vertical transport in graphene–hexagonal boron nitride heterostructure devices *Sci. Rep.* **5** 14519
[6] Glavin N R *et al* 2016 Amorphous boron nitride: a universal, ultrathin dielectric for 2d nanoelectronics *Adv. Funct. Mater.* **26** 2640–7
[7] Mayorov A S *et al* 2011 Micrometer-scale ballistic transport in encapsulated graphene at room temperature *Nano Lett.* **11** 2396–9
[8] Morozov S V, Novoselov K S, Katsnelson M I, Schedin F, Elias D C, Jaszczak J A and Geim A K 2008 Giant intrinsic carrier mobilities in graphene and its bilayer *Phys. Rev. Lett.* **100** 016602
[9] Dean C R *et al* 2010 Boron nitride substrates for high-quality graphene electronics *Nat. Nanotechnol.* **5** 722–6
[10] Lin Y C, Lu C C, Yeh C H, Jin C, Suenaga K and Chiu P W 2012 Graphene annealing: how clean can it be? *Nano Lett.* **12** 414–9
[11] Park J H, Choi S H, Chae W U, Stephen B, Park H K, Yang W, Kim S M, Lee J S and Kim K K 2015 Effective characterization of polymer residues on two-dimensional materials by Raman spectroscopy *Nanotechnology* **26** 485701
[12] Karlsson L H, Birch J, Mockute A, Ingason A S, Ta H Q, Rummeli M H, Rosen J and Persson P O A 2016 Residue reduction and intersurface interaction on single graphene sheets *Carbon* **100** 345–50
[13] Suk J W, Lee W H, Lee J, Chou H, Piner R D, Hao Y, Akinwande D and Ruoff R S 2013 Enhancement of the electrical properties of graphene grown by chemical vapor deposition via controlling the effects of polymer residue *Nano Lett.* **13** 1462–7
[14] Choi W, Seo Y S, Park J Y, Kim K B, Jung J, Lee N, Seo Y and Hong S 2015 Effect of annealing in Ar/H_2 environment on chemical vapor deposition-grown graphene transferred with poly (methyl methacrylate) *IEEE Trans. Nanotechnol.* **14** 70–4
[15] Song L, Liu Z, Reddy A L M, Narayanan N T, Taha-Tijerina J, Peng J, Gao G, Lou J, Vajtai R and Ajayan P M 2012 Binary and ternary atomic layers built from carbon, boron, and nitrogen *Adv. Mater.* **24** 4878–95
[16] Wang L *et al* 2013 One-dimensional electrical contact to a two-dimensional material *Science* **343** 614–7
[17] Vlassiouk I, Fulvio P, Meyer H, Lavrik N, Dai S, Datskos P and Smirnov S 2013 Large scale atmospheric pressure chemical vapor deposition of graphene *Carbon* **54** 58–67
[18] Stehle Y Y, Meyer H, Unocic R R, Kidder M, Polizos G, Datkos P, Jackson R K, Smirnov S and Vlassiouk I 2015 Synthesis of hexagonal boron nitride monolayer: control of nucleation and crystal morphology *Chem. Mater.* **27** 8041–7
[19] Ci L *et al* 2010 Atomic layers of hybridized boron nitride and graphene domains *Nat. Mater.* **9** 430–5
[20] Gao Y, Ren W, Ma T, Liu Z, Zhang Y, Liu W, Ma L, Ma X and Cheng H 2013 Repeated and controlled growth of monolayer, bilayer and few-layer hexagonal boron nitride on Pt foils *ACS Nano* **7** 5199–206
[21] Ferrari A C *et al* 2006 Raman spectrum of graphene and graphene layers *Phys. Rev. Lett.* **97** 187401
[22] Graf D, Molitor F, Ensslin K, Stampfer C, Jungen A, Hierold C and Wirtz L 2007 Spatially resolved Raman spectroscopy of single- and few-layer graphene *Nano Lett.* **7** 238–42
[23] Ni Z, Wang Y, Yu T and Shen Z 2008 Raman spectroscopy and imaging of graphene *Nano Res.* **1** 273–91
[24] Geim A K and Grigorieva I V 2013 Van der Waals heterostructures *Nature* **499** 419–25
[25] Nayfeh O M, Birdwell A G, Tan C, Dubey M, Gullapalli H, Liu Z, Reddy A L M and Ajayan P M 2013 Increased mobility for layer-by-layer transferred chemical vapor deposited graphene/boron–nitride thin films *Appl. Phys. Lett.* **102** 103115
[26] Fan Y, Zhao M, Wang Z, Zhang X and Zhang H 2011 Tunable electronic structures of graphene/boron nitride heterobilayers *Appl. Phys. Lett.* **98** 083103
[27] Loh G C and Pandey R 2015 A graphene–boron nitride lateral heterostructure—a first-principles study of its growth, electronic properties, and chemical topology *J. Mater. Chem.* C **3** 5918–32
[28] Vlassiouk I, Polizos G, Cooper R, Ivanov I, Keum J K, Paulauskas F, Datskos P and Smirnov S 2015 Strong and electrically conductive graphene based composite fibers and laminates *ACS Appl. Mater. Interfaces* **7** 10702–9